INFLUENCE OF MOLTEN SALT (FLINAK) THERMOPHYSICAL PROPERTIES ON A HEATED TUBE USING CFD RANS TURBULENCE MODELING OF AN EXPERIMENTAL TESTBED.

A Thesis

by

RAMIRO FREILE

Submitted to the Office of Graduate and Professional Studies of
Texas A&M University
in partial fulfillment of the requirements for the degree of

MASTER OF SCIENCE

Chair of Committee,	Mark L. Kimber
Committee Members,	Pavel V. Tsvetkov
	Michael Pate
Head of Department,	Michael Nastasi

August 2020

Major Subject: Nuclear Engineering

ABSTRACT

In a liquid fuel molten salt reactor key factor to consider upon its design is the strong coupling between different physics present such as neutronics, thermo-mechanics and thermal-hydraulics. Focusing on the thermal-hydraulics aspect, in support of potential reactor designs, it is required that the heat transfer is well characterized. For this purpose, turbulence models used for FLiNaK flow must be valid, and its thermophysical properties must be accurately described. In the literature, several expressions for each material property can be found, with differences that can be quite significant.

The goal of this study is to demonstrate and quantify the impact that the uncertainty in thermophysical properties has on key metrics of thermal hydraulic importance for MSRs, in particular on the heat transfer coefficient. In order to achieve this, CFD simulations using the RANS k-ω SST model were compared to published experiment data on molten salt. Various correlations for FLiNaK's thermophysical properties were used. It was observed that the spread in FLiNaK's thermophysical properties lead to a significant variance in the heat coefficient. Motivated by this, additional CFD simulations were done to obtain sensitivity coefficients for each thermophysical property. With this information, the effect of the variation of each one of the material properties on the heat transfer coefficient was quantified performing a one factor at a time approach.

The results of this sensitivity analysis showed that the most critical thermophysical properties of FLiNaK towards the determination of the heat transfer coefficient are the viscosity and the thermal conductivity. More specifically the dimensionless sensitivity coefficient, which is defined as the percent variation of the heat transfer with respect to the percent variation of the respective property, was -0.51 $\pm$ 0.07 and 0.64 $\pm$ 0.03 respectively. According to the different correlations, the maximum percent variations for these properties present in literature is 18% and 26% respectively, which yields a variation in the predicted heat transfer coefficient as high as 9% and 17% for the viscosity and thermal conductivity, respectively.

It was also demonstrated that the Nusselt number trends found from the simulations were cap-

tured much better using the Sieder Tate correlation than the Dittus Boelter correlation. Future work accommodating additional turbulence models and higher fidelity physics will help to determine whether the Sieder Tate expression truly captures the physics of interest or whether the agreement seen in the current work is simply reflective of the single turbulence model employed.

DEDICATION

To my family, for their inconditional support.

To all professors from Instituto Balseiro and Texas A&M who have contributed to my formation.

ACKNOWLEDGMENTS

I would like to thank my advisor Dr. Kimber and the members of my research group consisting of Corey Clifford, Austen Fradeneck, Adam Oler and Nolan MacDonald who assisted me in getting familiar with the needed tools for performing this work. Furthermore, I greatly thank Mauricio Tano for the talks we have had that assisted in the making of this thesis. I would also like to thank Gerrit Botha for his tutoring in DNS. In addition, I would like to thank the reviewers of EPJN (European Physical Journal Nuclear Sciences & Technologies) for their valuable contribution to the research performed.

CONTRIBUTORS AND FUNDING SOURCES

Contributors

This work was supported by a thesis committee consisting of Professor Mark Kimber and Professor Pavel Tsvetkov of the Department of Nuclear Engineering and Professor Michael Pate of the Department of Mechanical Engineering.

The Computational Fluid Dynamics (CFD) simulations were completed using ANSYS FLUENT v19.0 software. The licenses required to utilize this software were provided by Texas A&M University. The Texas A&M high performance computing clusters were used to perform the various CFD simulations.

The work conducted for the thesis was completed by the student independently.

Funding Sources

Graduate study was supported by graduate research from Texas A&M University under NuSTEM (Nuclear Science, Technology and Education for Molten Salt Reactors) project.

NOMENCLATURE

AMG	Algebraic Multi Grid
CFD	Computational Fluid Dynamics
DNS	Direct Numerical Simulations
LES	Large Eddy Simulations
MSR	Molten Salt Reactor
MSFR	Molten Salt Fast Reactor
OAT	One Factor at a Time Approach
Pr	Prandtl number
RANS	Reynolds Averaged Navier Stokes
Re	Reynolds number
SIMPLE	Semi-Implicit Method for Pressure Linked Equations
SST	Shear Stress Transport
VHTR	Very High Temperature Reactor

MATH SYMBOLS

k	Turbulent Kinetic Energy
ω	Turbulent Specific Dissipation Rate
ϵ	Turbulent Dissipation Rate
λ	Thermal Conductivity
cp	Specific Heat
ρ	Density
μ	Dynamic Viscosity
μ_t	Turbulent Viscosity
δ_{ij}	Cronecker Delta
u_i	Instantaneous velocity in direction i
U_i	Mean Velocity in direction i
$u_i^{'}$	Velocity Fluctuations in direction i
p	Instantaneous Pressure
P	Mean Pressure
$p^{'}$	Pressure Fluctuations
τ_{ij}	Fluid Stress Tensor
$-\overline{u^{'}{}_i u^{'}{}_j}$	Reynolds Stress Tensor
T	Temperature
$T^{'}$	Temperature Fluctuations
E	Energy
H	Enthalpy
Pr_t	Turbulent Prandtl Number

$-\overline{T' u_j'}$	Turbulent Heat Flux
Q'''	Volumetric Heat Flux
Q	Total Heat
α_t	Eddy diffusivity
y^+	Dimensionless Wall Distance
τ_w	Wall Shear Stress
ν	Kinematic Viscosity
T_{in}	Inlet Temperature
T_{out}	Outlet Temperature
T_b	Bulk Temperature
$T_w sim$	Simulation Wall Averaged External Temperature
$T_w exp$	Experiment Wall Averaged External Temperature
V^{avg}	Averaged Cross Sectional Integral of the velocity
S	Sensitivity Coefficient
S^*	Dimensionless Sensitivity Coefficient
h	Heat Transfer Coefficient

TABLE OF CONTENTS

Page

LIST OF FIGURES

FIGURE Page

LIST OF TABLES

TABLE Page

1. INTRODUCTION

During the last 50 years there has been a rising interest in the use of molten salts as a heat transfer fluid. In particular, they have been considered among the best candidates for the advanced reactor design of the Generation IV reactor concepts [1].

Molten salts' primary function in a nuclear reactor is to act as a coolant, extracting the heat resulting from the nuclear fission. These designs may have variations according to how the fuel is arranged in the core. For example, the fuel may be present in the form of a ceramic fuel in prisms or pebble bed (Liquid-salt-very-high-temperature reactor) or rather dissolved in the salt itself. A very promising design is the liquid-fueled molten salt reactor, which is the only concept of the Generation IV generation which employs a liquid fuel. Figure 1.1 shows a schematic representation of the European MSFR design. Fluorides of fissile and/or fertile elements such as UF4, PuF3 and/or ThF4 are combined with carrier salts to form fluids. The most famous carrier salt candidates are FLiNaK (46.5 LiF–11.5 NaF–42 KF mol%) and FLiBe (66 LiF-34 BeF2 mol%), the former having a higher solubility for fissile fluorides. The heat generated in the molten salt is transferred to a secondary coolant system through an intermediate heat exchanger, and then through a tertiary heat exchanger to the power conversion system. The system has a coolant outlet temperature of $700\,^{\circ}\mathrm{C}$, possibly ranging up to $800\,^{\circ}\mathrm{C}$, affording improved thermal efficiency.

Molten salt reactors designed with liquid fuels have numerous operational and safety advantages over solid fuel designs.

- Homogeneity of the fuel makes it unnecessary to account for a loading plan.
- Fluoride salts present a high solubility for uranium, are chemically stable, have very low vapor pressure, have high specific heat, are resistant to radiation, and are inert to some common structural metals.
- Meltdown does no longer represent a safety issue, and the fuel may be automatically drained to a passively cooled, critically safe dump tank when facing a sudden power rise.

- Fission products may form stable fluorides that will stay within the salt during any leak or accident. There is a continuous removal of noble gases and other fission products, meaning that Xenon build up will not produce any "dead time" after shutdown.

- Most MSR designs have very strong negative temperature and void coefficients which act instantly, enabling the reactor to be inherently safe with changes in power.

In a MSR a key factor towards its modeling is the strong coupling between the physics describing the neutronics and the thermal-hydraulics. The velocity field affects the neutron precursors transport and the temperature field affects the neutron population through Doppler effects and density changes in the coolant. Hence, it is of paramount importance to be able to describe the fluid flow and the thermal characteristics of the molten salt fluid. In order to do so, it is required that the turbulence models used are valid for the molten salt flow and that the thermophysical properties are accurately described.

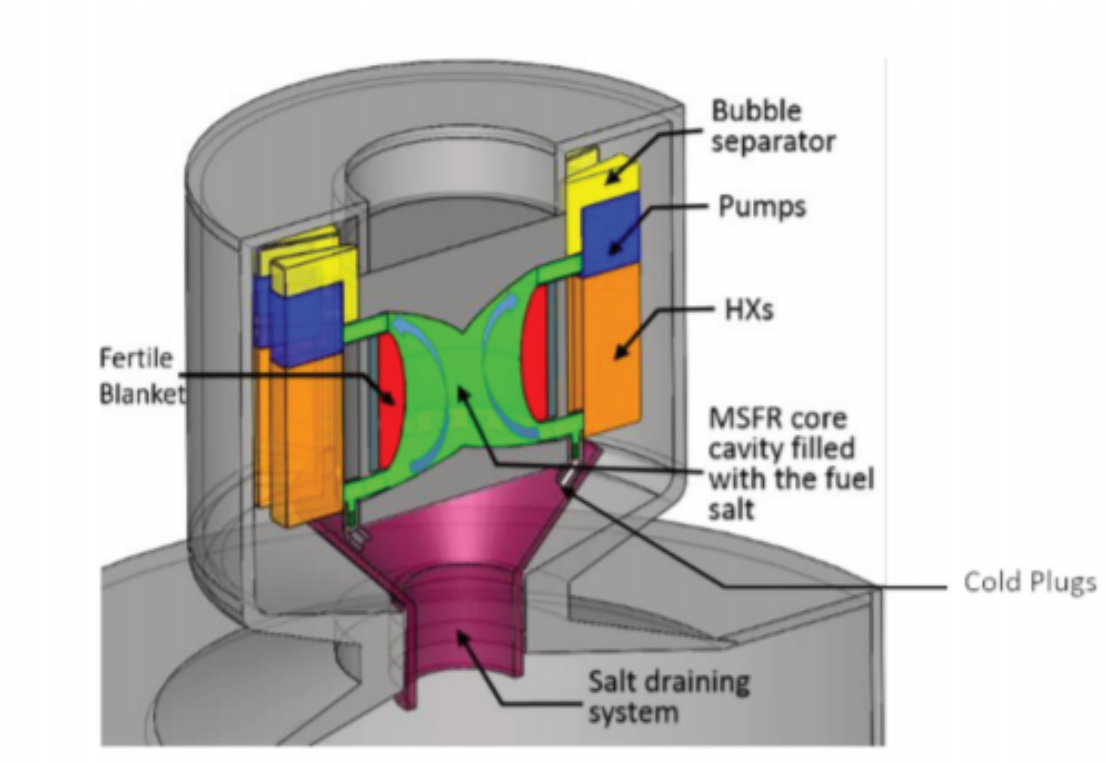

Figure 1.1: Schematic representation of the primary circuit of the MSFR. Figure taken from [2]

2. PREVIOUS RESEARCH AND MOTIVATION

2.1 Previous Research

Historically, the investigation of molten salts began in the late 1950s at Oak Ridge National Laboratory, aimed at the development of a molten-salt nuclear reactor to power an airplane. In 1954 the first molten salt reactor for the Aircraft Reactor Experiment was built at Oak Ridge to investigate the use of molten fluoride fuels for an aircraft propulsion reactor.

During the same time period, forced convection experiments were performed to examine heat transfer properties of molten salts, in particular FLiNaK. In 1954 Grele and Gedeon [3] and Hoffman and Lones [4] [1] performed experimental measurements using FLiNaK flowing through a heated test section with different piping materials. Nusselt numbers were calculated and contrasted with the Dittus-Boelter correlation, depicting an underprediction of about 50% in value. Final results revealed good agreement when using Ni and SS316, but as much as 50% of underprediction using Inconel. The results obtained by these experimentalists is shown in Figure 2.1.

[1] Part of the data reported in this chapter is reprinted with permission from "J. Ambrosek, M. Anderson, K. Sridharan & T. Allen (2009) Current Status of Knowledge of the Fluoride Salt (FLiNaK) Heat Transfer, Nuclear Technology, 165:2, 166-173, DOI: 10.13182/NT165-166". Copyright 2009 by Informa UK Limited.

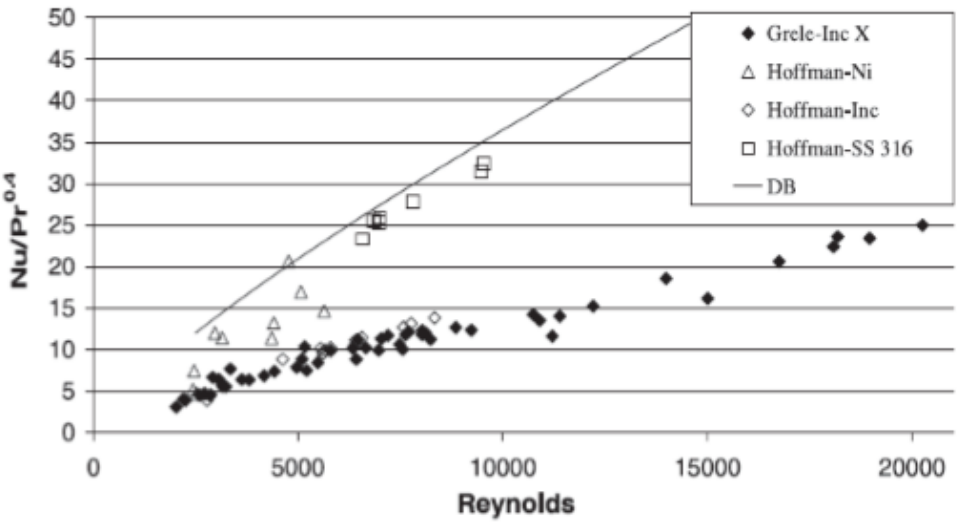

Figure 2.1: Experimental results obtained by Grele and Gedeon [3] and Hoffman and Loans [4] compared with Dittus Boelter correlation

Later in the 1970's, Vriesema performed measurements on forced convection in a vertical pipe [5]. The results of Nusselt number were 15% off the Dittus Boelter prediction, as shown in Figure 2.2.

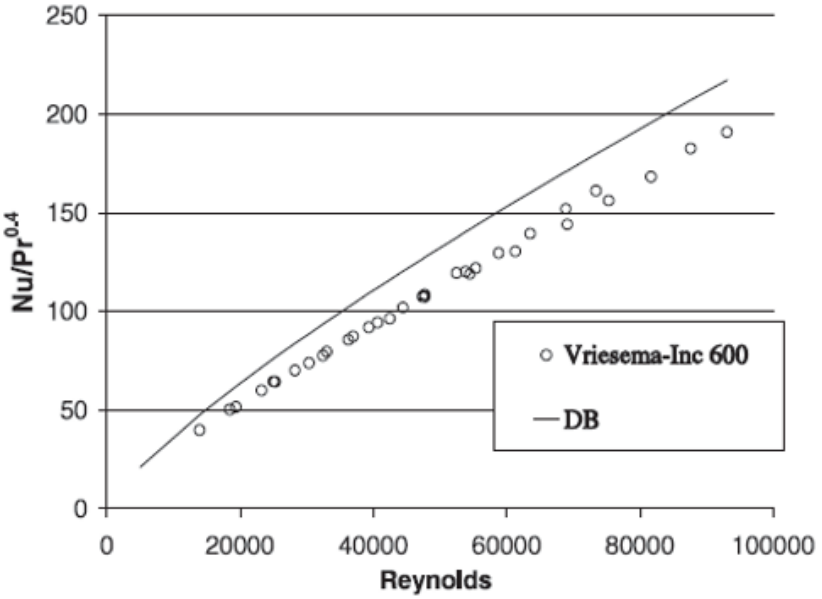

Figure 2.2: Experimental results obtained by Vriesema[5] compared with Dittus Boelter

Ignat'ev et al. [6] also performed heat transfer studies using FLiNaK in a circular tube of iron-based steel. The results were compared with the Petukhov-Kirillov formula, yielding a maximum error of 10% with respect to their experimental data.

Throughout all these experiments appearing in the literature, they all had the common problem of not knowing precisely the value of the thermophysical properties of the molten salt. In particular, the wide range of values adopted by these researchers for thermal conductivity is worth noting. For FLiNaK, Grele and Gedeon and Hoffman and Loans used for their Nusselt calculations a thermal conductivity of $\lambda = 4.5\frac{W}{m\cdot K}$, while Vriesema used $\lambda = 1.3\frac{W}{m\cdot K}$. In the Grele and Gedeon report it was mentioned that the reason for the huge discrepancy between their measurements and Dittus Boelter was due to the formation of a film associated with the chromium that was corroded from the Inconel piping, resulting in an additional resistance to heat transfer in the Inconel tube. Studies done by [9] suggest that another possible reason for the existent large discrepancy was the adopted value of FLiNaK's thermal conductivity.

Experimentally determining thermal conductivity for molten salts is a challenging task, as it is necessary to differentiate the contributions from the radiation, natural convection and conduction heat transfer modes in a given experiment [7] [9]. Because the thermal conductivity values in the past overestimated by a factor of 4 the most widely accepted values nowadays [8], it can be argued that all the heat transfer modes were not taken into account during the thermal conductivity measurements in that era.

In 1962, Ewing [7] was the first to realize that the thermal radiation in molten salts could significantly affect the experimental measurements for the conductivity. He described the measured value as an effective thermal conductivity, accounting for a molecular conduction plus a thermal radiation conduction. Ewing concluded that the effective thermal conductivity values were very sensitive to the conditions of the experiment. In his measurements, the FLiNaK conductivity values ranged from $0.6\frac{W}{m\cdot K}$ to $5\frac{W}{m\cdot K}$. The former was constant during each run equal to $\lambda = 0.6\frac{W}{m\cdot K}$.

Another set of experiments found in literature for measuring the thermal conductivity of FLiNaK was done by Smirnov [8] in 1987. He used the method of coaxial cylinders made of platinum,

with radiation heat transfer taken into account. He proposed an empirical correlation for the thermal conductivity equal to $\lambda = 0.36 + 0.00056.T\frac{W}{m\cdot K}$ over the range of $517\,^{\circ}\mathrm{C}$ to $817\,^{\circ}\mathrm{C}$.

In 2009, Ambrosek [9] [2] reanalyzed each of the previously mentioned experiments using the most widely accepted thermophysical properties of FLiNaK. In particular, he used Smirnov's correlation, and found thermal conductivity values of λ=0.81-0.93 $\frac{W}{m\cdot K}$ over the temperature range of validity. The final result of this analysis agreed within 15 % with respect to Dittus Boelter correlation for Inconel piping. The reanalyzed data by Ambrosek is shown in Figure 2.3. Even though in this figure, the results for Ni and SS316 pipes was not shown, it must be said that they presented a large discrepancy when compared with the Dittus Boelter correlation. No explanation could be found for these results.

After this work done by Ambrosek, it was concluded that the main reason why the first experimentalists had observed results in great discordance with the known correlations was the misprediction in the thermal conductivity of FLiNaK used for their calculations.

[2] Part of the data reported in this chapter is reprinted with permission from "J. Ambrosek, M. Anderson, K. Sridharan & T. Allen (2009) Current Status of Knowledge of the Fluoride Salt (FLiNaK) Heat Transfer, Nuclear Technology, 165:2, 166-173, DOI: 10.13182/NT165-166". Copyright 2009 by Informa UK Limited.

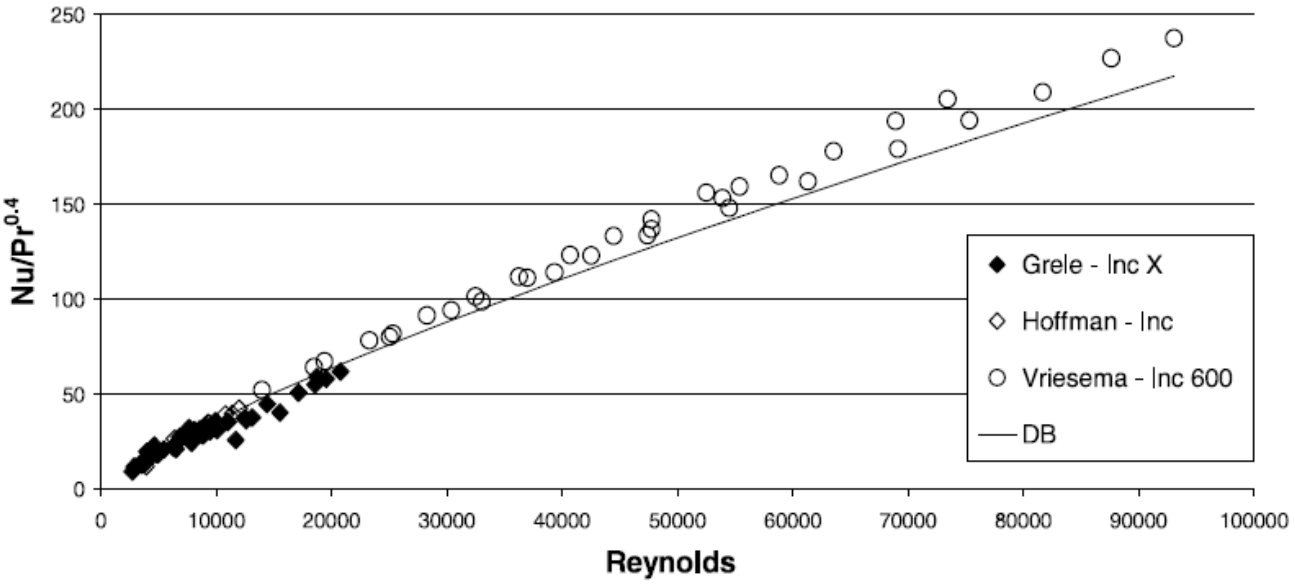

Figure 2.3: Grele and Gedeon, Hoffman and Loans and Vriesema results for Inconel piping reanalyzed by Ambrosek et al. [9]

In 2013, Idaho National Laboratory published an Engineering database of liquid salt thermophysical properties [10]. It consists of a compilation of the different commonly accepted correlations for the temperature dependent FLiNaK properties such as specific heat, density, viscosity and thermal conductivity. In Table 2.1 some of the most widely accepted correlations for these properties are shown. Note that for the thermal conductivity there is only one expression in the table, which is the most widely accepted temperature dependent expression. However, according to studies done by Williams et al. [13], the thermal conductivity value should range between $0.6\frac{W}{m\cdot K}$ and $1.0\frac{W}{m\cdot K}$ at 973 K.

Table 2.1: Correlations for thermophysical properties of FLiNaK taken from [10]

Thermophysical property	**Correlation**	**Reference**
Specific Heat[$\frac{J}{kg.K}$]	$cp_1 = 976.8 + 1.0634.T$	[13]
	$cp_2 = 1,905$	[15]
Density[$\frac{kg}{m^3}$]	$\rho_1 = 2,555 - 0.6.T$	[3], [4]
	$\rho_2 = 2,729 - 0.73.T$	[5]
Thermal Conductivity[$\frac{W}{m.K}$]	$\lambda_1 = 0.36 + 5.6 \times 10^{-4}.T$	[13]
	$\lambda_2 = 0.6$	[13]
	$\lambda_3 = 1.0$	[8]
Dynamic viscosity [Pa.s]	$\mu_1 = 4 \times 10^{-5}.exp(4,170.T)$	[9]
	$\mu_2 = 2.5 \times 10^{-5}.exp(4,790/T)$	[3], [4]
	$\mu_3 = 1.1 \times 10^{-4}.exp(3,379/T)$	[5]
	$\mu_4 = 2.49 \times 10^{-5}.exp(4,478.6/T)$	[14]

As noted earlier, it is unclear which set of expressions would be best to use. With this in mind, the authors in [10] determined the effect of uncertainty in the resulting Nusselt number, but assumed complete validity of the Dittus Boelter equation. For the worst case scenario, the maximum reported error due to thermophysical uncertainties in the Nusselt number was +/- 8%. However, those authors suggested a more detailed analysis should be conducted, one that does not rely on Nusselt number correlations or the assumption of constant properties.

In the scientific community other efforts were made to perform sensitivity analysis of heat transfer in molten salts. Xu et al. [11] conducted a sensitivity study of heat transfer mechanisms in a packed-bed molten salt thermocline thermal storage system using a two-phase model. Different interstitial heat transfer correlations, which are functions of the Reynolds number and the porosity, were used to compare the thermal performance of the storage system. Sabharwall et al. [12] performed hand-made calculations of the sensitivity coefficients for the different thermophysical

properties in the VHTR. In their calculations, an analytical equation for the heat transfer coefficient was obtained by using the Dittus Boelter equation and using a fixed pressure drop with friction coefficients for the velocity estimation, which was made using the Blasius formula. Partial derivatives of the heat transfer coefficient with respect to each individual thermophysical property were taken and dimensionless sensitivity coefficients were obtained. Therefore, in the calculation of the sensitivity coefficients, they assumed that Dittus Boelter is valid and that the bulk temperature of the salt does not strongly depend on the molten salt properties.

2.2 Contribution

To the best of our knowledge, there is no definitive expression that best defines molten salt material properties, particulary FLiNaK's properties. Several expressions for each material property are found in the literature, with noticeable differences in the values one would predict. In addition, properties such as viscosity and thermal conductivity have a considerable uncertainty in experimental measurements.

As a consequence of the limitations just mentioned, in order of importance, this work's contribution aims at:

- Quantifying the impact that the spread in molten salt's thermophysical properties present in literature has on the pertinent thermal hydraulics. This will support future experiments efforts, helping to gain a notion on the level of accuracy needed to produce high quality data.

- Obtaining sensitivity coefficients for each thermophysical property. This information provides a good estimate on how much variation in the heat transfer coefficient is expected as a consequence of a variation in the property itself and determine which is the most influential property. With this coefficient, the effect of the uncertainties in the experimental measurements of a certain property on the heat transfer coefficient is reflected.

- Assessing the adequacy of different Nusselt number correlations including Dittus Boelter and Sieder Tate.

For this purpose, the present work implements computational fluid dynamics as a tool to obtaining sensitivity coefficients for each material property and assess the effect of the spread in thermophysical properties, which has been a problematic that researchers have had along these years (see 2.1). The simulations are carried out in accordance with a published experiment on molten salt FLiNaK done by Grele and Gedeon [3]. Simulation results for different combinations of thermophysical properties are compared to the experiment.

3. GRELE AND GEDEON EXPERIMENT

In 1954, Grele and Gedeon conducted an experiment in a FLiNaK molten salt loop to compute the Nusselt number and contrast it with Dittus Boelter. The test section, where the pertinent measurements were taken, is shown in Figure 3.1.

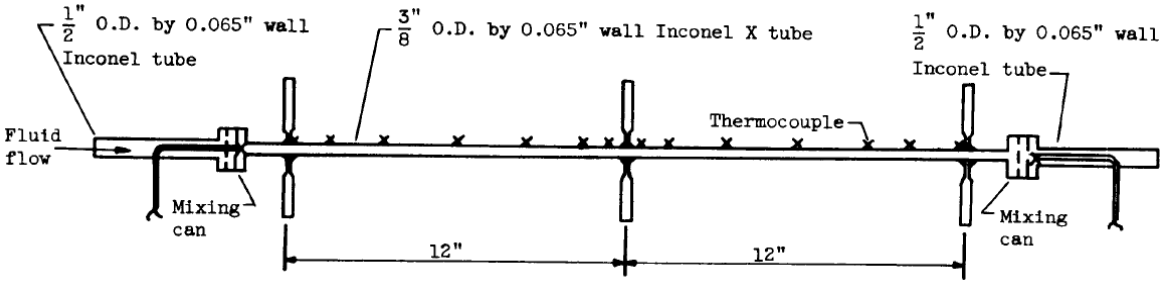

Figure 3.1: Sketch of the experimental setup used by Grele and Gedeon [3].

The pipes in the test section were made of Inconel X with an outside diameter of 3/8 inches and a wall thickness of 0.065 inches. The length was 24 inches. Electric heaters were fixed around the pipe circumference and provided the required heating. Two mixing cans were positioned before and after the test section to provide inlet and outlet temperatures via a thermocouple in each location. Fourteen additional thermocouples were placed along the outside wall of the test pipe at different axial locations to measure the outside wall temperature.

The wall temperature that was reported in each one of the runs was an average of the measurement coming from twelve thermocouples, ignoring the temperature values of the two thermocouples at the two ends of the pipe. The mass flow in each run was obtained using a volume-measuring tank located within the loop. The fluid level rose in the tank and upon reaching the first of a pair of contact points an electric stopwatch was started. When the level reached the second contact point, which was located at a known distance above the first, the clock was stopped, which enabled calculation of the average velocity.

Apart from the wall temperature, the velocity and the inlet and outlet temperature, other quantities such as internal surface temperature, heat flux, mass flow, were reported. It is important to highlight that these other quantities were derived using Grele and Gedeon's expressions for FLiNaK's thermophysical properties. For example, the heat applied to the test section was calculated using energy balance between the inlet and outlet, which required expressions for the specific heat and density. With this information and the thermal conductivity of Inconel X, the internal surface temperature was calculated. This is the reason why, for each choice of thermophysical properties, the effective heat applied will change accordingly. The inlet and outlet temperature, the wall temperature and the velocity inlet are independent of their choice of correlations for FLiNaK's properties. The first three of these are directly measured and therefore require no explanation as to their attribute of being independent of which fluid properties are assumed. The last of these (average velocity), although not directly measured, can easily be shown to be property independent through a simple mass balance analysis.

4. GOVERNING EQUATIONS AND MODELING

4.1 Fluid dynamics

The set of equations describing the physics of any compressible Newtonian fluid flow are the continuity equation and the momentum balance or Navier Stokes equations:

$$\frac{\partial \rho}{\partial t} + \frac{\partial}{\partial x_i}\left(\rho u_i\right) = 0 \tag{4.1}$$

$$\frac{\partial (\rho u_i)}{\partial t} + \frac{\partial}{\partial x_j}\left(\rho u_i u_j\right) = -\frac{\partial p}{\partial x_i} + \frac{\partial \tau_{ij}}{\partial x_j} \tag{4.2}$$

$$\tau_{ij} = \mu\left(\frac{\partial u_i}{\partial x_j} + \frac{\partial u_j}{\partial x_i}\right) - \frac{2}{3}\mu\delta_{ij}\frac{\partial u_k}{\partial x_k} \tag{4.3}$$

It must be clarified that the compressibility effect (change in the density of the fluid) can be caused either by temperature or by pressure. In the case of molten salt flow in a pipe, from the standpoint of view of the pressure influence on the density, it can be said that it will remain constant. The way to justify this statement is by analyzing the Mach number, which in this particular case is much lower than one. On the other hand, in heated flows, there will be a density variation due to its dependence on temperature. Although the dilatation term on the right of Equation 4.3 was modelled, it can be said that its value will still be negligible compared with the rate of strain tensor.

4.2 Turbulence Modeling

Depending on the type of flow modelled and parameters such as the geometry, mean flow velocity and thermophysical properties of the fluid, the momentum equation can describe different types of flow regime. In order to determine this regime, the Reynolds number, which is a dimensionless parameter defined as a ratio of the inertial forces over the viscous forces, is used. For

Reynolds numbers lower than 2300, the flow can be described as a group of fluid layers sliding one with another. This type of stable regime is called laminar flow. When the Reynolds number is high (Re>4000) the flow becomes chaotic, entering in a turbulent regime. This type of regime, characterized by flow fluctuations of different sizes and periods, (called eddies) arising from the nonlinearity of Navier Stokes equation, favors momentum exchange, Therefore, energy transfer from the walls to the bulk is enhanced. For this reason, considering the application of heat exchangers or even the molten salt reactor, turbulent flow regime is preferred.

Turbulence is a complex phenomenon with important temporal and spatial scales that exist across many orders of magnitude. Therefore, the modeling of all these scales becomes computationally expensive, making it not viable for sensitivity analyses, which require a large amount of simulations. Thus, most modeling approaches rely on one or many flow assumptions that simplify the path to a solution.

In this work, equations of flow motion were solved using the Reynolds Averaged Navier Stokes models. Using this approach, the instantaneous velocity is expressed as the sum of a mean velocity $U_i\left(x\right)$, and a fluctuating part, $u^{'}{}_i\left(x,t\right)$, such that:

$$u_i\left(x,t\right) = U_i\left(x\right) + u^{'}{}_i\left(x,t\right) \tag{4.4}$$

where

$$U_i\left(x\right) = \lim_{T\to\infty} \frac{1}{T} \int_t^{t+T} u_i\left(x,t\right) dt$$

Analogously, the pressure can be also decomposed as a mean pressure and a fluctuating pressure:

$$p\left(x,t\right)=P\left(x\right)+p^{'}\left(x,t\right) \tag{4.5}$$

Replacing the instantaneous velocity in the Navier Stokes equations, and time averaging both yields the Reynolds averaged equations of motion:

$$\frac{\partial\rho}{\partial t}+\frac{\partial}{\partial x_i}\left(\rho U_i\right)=0 \tag{4.6}$$

$$\frac{\partial(\rho U_{_i})}{\partial t}+\frac{\partial}{\partial x_j}\left(\rho U_i U_j\right)=-\frac{\partial P}{\partial x_i}+\frac{\partial}{\partial x_j}\left[\mu\left(\frac{\partial U_i}{\partial x_j}+\frac{\partial U_j}{\partial x_i}\right)-\frac{2}{3}\mu\delta_{ij}\frac{\partial U_k}{\partial x_k}\right]+\frac{\partial}{\partial x_j}(-\rho\overline{u^{'}{}_i u^{'}{}_j}) \tag{4.7}$$

The last term on the right hand side of Equation 4.7 represents the effects of turbulence on the mean flow and it is commonly known as the Reynolds stress tensor. Note that for this Reynolds stresses an overbar is used to denote the time averaged quantities of those variables. These Reynolds stresses must be modeled in order to close the equations. In this work, the Boussinesq approximation was used. The expression for the Reynolds tensor using this approximation is shown in the next equation:

$$-\rho\overline{u^{'}{}_i u^{'}{}_j}=-\frac{2}{3}k\delta_{ij}+\mu_t\left(\frac{\partial U_i}{\partial x_j}+\frac{\partial U_j}{\partial x_i}\right) \tag{4.8}$$

where *k* is defined as the turbulent kinetic energy $k=\frac{1}{2}\overline{u^{'}{}_i u^{'}{}_i}$ and μ_t is the turbulent viscosity, whose expression varies accordingly to the model used.

In this work a two-equation model was used. In these types of models the turbulent viscosity μ_t is taken as a function of the turbulent kinetic energy and the turbulent dissipation $\epsilon=\nu\overline{\frac{\partial u^{'}{}_i}{\partial x_k}\frac{\partial u^{'}{}_i}{\partial x_k}}$. Particularly for this work, the *k*-ω SST model was used, where $\omega=\frac{\epsilon}{k}$ is called specific dissipation or turbulent frequency.

The difference of two-equation models with the one-equation model and the zero-equation

model is that for the estimation of the turbulent viscosity μ_t, k and ω are obtained from actual equations and not by using weak assumptions. Thus, besides Equations 4.6 and 4.7, an equation is derived for the turbulent kinetic energy and the specific dissipation. In particular, for the k-ω SST model:

$$\frac{\partial(\rho k)}{\partial t} + \frac{\partial}{\partial x_i}(\rho k U_i) = \frac{\partial}{\partial x_j}\left(\Gamma_k \frac{\partial k}{\partial x_j}\right) + \widetilde{G_k} - Y_k \tag{4.9}$$

$$\frac{\partial(\rho \omega)}{\partial t} + \frac{\partial}{\partial x_i}(\rho \omega U_i) = \frac{\partial}{\partial x_j}\left(\Gamma_\omega \frac{\partial \omega}{\partial x_j}\right) + G_\omega - Y_\omega + D_\omega \tag{4.10}$$

where $\widetilde{G_k}$ represents the generation of turbulence kinetic energy, G_ω represents the generation of ω, $\Gamma_{(k/\omega)} = \mu + \frac{\mu_t}{\sigma_{(k/\omega)}}$ represent the effective diffusivity of k or ω, $Y_{(k/\omega)}$ describes the dissipation of k or ω due to turbulence and term D_ω represents the cross-diffusion term arising from the blending of the k-ω and k-ϵ models.

The shear-stress transport (SST) k-ω model was developed by Menter [16] with the objective of combining two of the most popular two-equation models, k-ω and k-ϵ, through the use of blending functions. Both of the aforementioned models are multiplied by a blending function and both models are added together. The blending function is generally a hyperbolic tangent whose range is restricted between zero and one. It is designed in such a way that near the wall, the standard k-ω model is predominant, and zero away from the surface, which activates the k-ϵ model in the free stream region. By doing this, the k-ω SST model is directly usable all the way down to the wall through the viscous sub-layer, hence being able to resolve turbulent parameters up to the wall region. In addition, in the free stream region it avoids the common k-ω problem of being overly sensitive to the inlet free stream turbulence properties and takes advantage of the k-ϵ model's advantage for free-shear flows.

There are several works which have been done on the CFD RANS modeling of molten salts.

Ferng et al. [21] proposed a CFD methodology for investigating thermal-hydraulic characteristics of FLiNaK in a pipe geometry using k-ϵ model. Results were compared to existing correlations. Chen et al. [20] performed calculations of Nusselt numbers for Hitec molten salt using four different RANS models and compared them with a present experiment of Hitec and several other experiments with different salts.

This turbulence model was chosen because of the good performance it has shown in other simulations related to the geometry of interest (i.e., pipe flow or channel flow). Kim et al. [17] investigated the effects of non-uniformity of fluid properties on forced convection heat transfer using different turbulence models by comparing against experiments. In this study, the effect of the non-uniformity of fluid properties was accounted for by applying a factor to the value of the Nusselt number for constant properties. The prediction with the k-ω model formulation was in good agreement with the experimental results. Menter et al. [18] compared the performance of the k-ω SST model in heat transfer applications with other turbulence models such as Low-Re models and k-epsilon models against experiments for different geometries. The best overall performance was achieved with the k-ω SST model. Given the conclusions of these two studies, the k-ω SST model is employed in the current work as well.

4.3 Heat Transfer

Similarly to what was shown in Equation 4.4, the energy *E* and enthalpy *H* are also decomposed into a mean and a fluctuating value. In order to compute the temperature distribution in the fluid (Equation 4.11) and in the solid (Equation 4.12), the equations of energy conservation were used:

$$\frac{\partial(\rho_f E_f)}{\partial t} + \frac{\partial}{\partial x_i}\left[U_i\left(\rho_f E_f + p\right)\right] = \frac{\partial}{\partial x_j}\left(\lambda_f \frac{\partial T_f}{\partial x_j} - \rho_f c_{p_f}\overline{T_f{}' u_j'}\right) \tag{4.11}$$

$$\frac{\partial(\rho_s H_s)}{\partial t} = \frac{\partial}{\partial x_j}\left(\lambda_s \frac{\partial T_s}{\partial x_j}\right) + Q''' \tag{4.12}$$

where $E = H - \frac{P}{\rho}$, $H = \int_{T_{ref}}^{T} c_p dT$ and Q''' is defined as a volumetric heat source in the solid. The term $\rho c_p \overline{T' u_j'}$ is commonly known as the turbulent heat flux.

In order to model this last term, a similar concept to the one used in Boussinesq approximation (Equation 4.8) is used:

$$-\rho c_p \overline{T' u_j'} = \alpha_t \frac{\partial T}{\partial x_j} = \frac{\mu_t}{Pr_t}\frac{\partial T}{\partial x_j} \tag{4.13}$$

where α_t is the eddy-diffusivity and Pr_t is the turbulent Prandtl number. This number was given a generally used constant value of 0.85 for the simulations [16].

Regarding radiation effects, results provided by Ambrosek et al. [9] proved that, because of the transparency of FLiNaK [7], the amount of energy transferred by radiation can be significant in applications involving high temperatures (T = 1123 K) and laminar flow conditions (Re < 500) in pipes with a diameter of 1 cm or greater. In the current experimental configuration, the pipe diameter is too small to take into account radiation heat transfer, as the convective heat transfer coefficient prevails over the radiative one. This was also proven by Ethan S. Chaleff et al. [23].

5. METHODOLOGY

5.1 Computational Domain

RANS simulations were carried out in this study using the finite volume CFD code ANSYS Fluent v19.0 commercial package. For this work the *k*-ω SST model was used for reasons previously noted. CFD codes require generating a computational domain and mesh to simulate flow behaviors in a specific geometry. The computational domain modeling the experimental test section in Grele and Gedeon experiment [3] was completed using ICEM CFD 19.0. The computational domain is shown in Figure 5.1.

The model consisted of a solid volume modeling the Inconel X pipe wall and a fluid volume to represent the molten salt flow. The diameters, the pipe wall thickness and the test section's length dimensions were in agreement with the test section used in [3]. Specifically, it had an outside diameter of 3/8 inches and a wall thickness of 0.065 inches. The total length of the computational domain was 24 inches.

A mesh convergence study using Richardson extrapolation [19] was made to assure that the model was producing a mathematically accurate solution. The number of elements was gradually increased until the wall temperature error for the highest Reynolds number case was below 1×10^{-2} K. The final total number of elements in the mesh was 1,054,585. The minimum orthogonal quality was 5.14×10^{-1} and the maximum aspect ratio was 50.4 in the cells which are the nearest to the wall. As seen in Figure 5.1, in the radial direction a 30x30 uniform square cartesian grid was used at the center of the pipe. The vertices of the square were equidistant from the origin at a distance of 1.8 mm. Thirty additional radial layers of cells exist between the bounds of the

square and the inner diameter of the pipe. A growth ratio of 1.005 from the wall was imposed in this section, and the first mesh division was set at 2×10^{-6} m. This refinement in the fluid region near the wall was made so that the model could resolve the equations for the temperatures and velocities up to the viscous sub-layer. In internal flows, the distance from the wall is generally represented by using the y^+ coordinate, which is defined as $y^+ = \frac{y \cdot \sqrt{\frac{\tau_w}{\rho}}}{\nu}$, where y is the distance from the wall and τ_w is the wall shear stress. For the highest Reynolds case, the mesh contained at least one grid point below normalized wall distance, i.e $y^+ = 1$, and at least five grid points in the viscous sublayer region, i.e. $y^+ = 5$. In the solid region, 8 equidistant divisions were imposed radially. In the axial direction, two hundred uniformly spaced divisions were imposed.

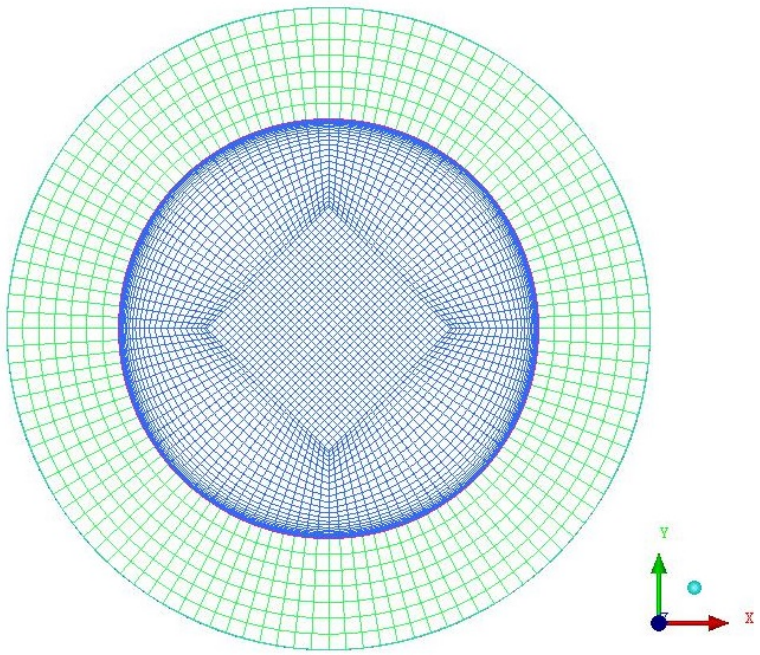

Figure 5.1: Perpendicular section of the computational domain used in the simulations

5.2 Numerical Schemes

The spatial discretization of the Reynolds Averaged Navier Stokes Equation has been done using the finite volume technique. Each simulated case was considered stationary, i.e. the temporal derivative was neglected. The discretization of the advective terms in the momentum, turbulent kinetic energy, dissipation and energy equation has been done using a second order upwind scheme, which takes information from the cell-center value and gradient value in the upstream cell. The gradients were computed by using the Green-Gauss Cell-Based method, which is taken from an average of the values at the neighboring cell centers in a certain direction. The pressure-velocity coupling within the RANS equations was obtained using the SIMPLE algorithm [22] using a second-order interpolation of the face flux via the method of Rhie and Chow. In a sequential manner, all transport equations were solved iteratively using the AMG solver. The simulations were considered converged once the normalized residuals levels became lower than 1×10^{-8}.

5.3 Boundary Conditions

5.3.1 Hydrodynamics

The boundary conditions applied to the numerical model include standard hydrodynamic conditions for pipe flow as well as thermal boundary conditions in both the fluid and solid regions of the model. The hydrodynamic boundary conditions are provided in Table 5.1, and include a prescribed hydrodynamically-developed velocity at the inlet, pressure outlet and no slip conditions at the wall. The inlet velocity is reported in [3], and was experimentally determined for each trial by measuring the amount of time it took for the fluid level to rise from one level to another in a volume-measuring tank locate d within the loop. Those authors used a pair of contact points and an electric stopwatch to make this calculation. The turbulence inlet boundary conditions were inputted

by using standard expressions for a fully developed internal flow, defining turbulence intensity and a reference length.

Table 5.1: Hydrodynamic boundary conditions used

Surface	Type	Description	Specifications
Inlet	Velocity inlet	Velocity inlet boundary conditions are used to define the flow velocity at flow inlets. The pressure is not fixed, but will change to whatever value is necessary to provide the prescribed velocity profile.	$U_x = 0$ $U_y = 0$ $U_z = case\ dependent$
Outlet	Pressure outlet	A gauge pressure is specified at the outlet. The velocity gradients are fixed to zero.	p = fixed arbitrary value
Wall	Wall	No-slip condition is imposed.	$U_i\|_{wall}$ =0

5.3.2 Energy

Solving the energy equation also required appropriate boundary conditions to be defined and are needed for both the fluid and the solid within the domain. These are shown in Table 5.2 and Table 5.3, respectively. The fluid inlet temperature for each trial is taken from [3] and the outlet is considered adiabatic. At the surface between the molten salt and the solid tube wall, an interface condition is applied which serves to thermally couple the two element types (i.e., solid and fluid). For the solid, this interface condition is also applied, while the remaining solid surfaces are all adiabatic. The coupled boundary condition was set in the interface. The solution for the temperatures in the interface are solved for by using the information of the temperatures of the interface adjacent cells, iterating until the energy balance is satisfied at the interface.

Table 5.2: Energy boundary conditions used for the fluid region

Surface	**Type**	**Specifications**
Inlet	Dirichlet	T_{in} = *case dependent*
Outlet	Neumann	*Heat Flux=0 (adiabatic)*
Wall	Interface	Coupled thermal conditions between fluid and solid regions. The solver will calculate heat transfer directly from the solution in the adjacent cells

Table 5.3: Energy boundary conditions used for the solid region

Surface	**Type**	**Specifications**
Inlet	Neumann	*Heat Flux=0 (adiabatic)*
Outlet	Neumann	*Heat Flux=0 (adiabatic)*
External surface	Neumann	*Heat Flux=0 (adiabatic)*
Internal surface	Interface	Coupled thermal conditions between fluid and solid regions. The solver will calculate heat transfer directly from the solution in the adjacent cells

Enhanced wall treatment was used during the simulations, which means that for the dimensionless velocity, a blending function is used to smoothly merge both the log layer and the viscous layer. For the thermal formulation, an elliptic blending is also used for merging the laminar and logarithmic profiles accordingly.

In Grele and Gedeon experiment, electrical heaters were fixed around the pipe circumference which provided the required heating. To model this, cell zone conditions were imposed in the solid region in order to add the volumetric heat source due to electrical heating. The constant volumetric heat source may have discrepancies with the actual experiment because of several factors such as non-uniformity of the electrical current and because of the variation of the pipe temperature.

However, because of the lack of data regarding the heat flux profiles, it was decided that the constant volumetric heat source was the best choice for reproducing the experiment as it represents the simplest solution for applying the thermal load.

In each one of the cases, the total heat supplied to the fluid was computed using the temperatures at the inlet and the outlet together with the choice of material properties (Table 2.1), particularly density and specific heat. The formula used was the following:

$$\rho^{x}(T_b).{c_p}^{y}(T_b).V^{avg}.A.(T_{out} - T_{in}) = Q^{xy} \tag{5.1}$$

where superscripts *x* and *y* refer to the different possibilities of thermophysical properties (Table 2.1), T_b is the bulk temperature calculated as $T_b = \frac{(T_{out}+T_{in})}{2}$ and *A* is the cross- sectional area of the pipe. After the total heat supplied to the fluid was computed, using the assumption of uniformly distributed heat, the volumetric heat source was inputted as a cell zone condition in the solid region.

6. CFD SIMULATION RESULTS AGAINST EXPERIMENT

6.1 Simulation Parameters

In order to assess the RANS models for molten salt flows (FLiNaK) and the effect of the spread in FLiNaK's thermophysical properties, different cases in the Grele and Gedeon experiment were simulated and compared to their experimental results. In the experiment, the external average wall temperature was reported in each run, which was found by simply averaging the 12 thermocouples located on the pipe wall at different axial positions. The wall temperature in the external wall of the modeled solid pipe at each one of the thermocouples' positions was averaged in order to directly compare with the reported external wall temperature from the experiment.

The thermophysical properties of FLiNaK were considered as temperature dependent in the simulations, implemented as user defined functions in Fluent. Due to the several expressions for FLiNaK material properties, for each case, different combinations of the material properties, previously presented in Table 2.1, were used. The thermal conductivity used was given by Smirnov's correlation, as the majority of the published literature consider this correlation as the most accurate for FLiNaK. In regards to the solid region, the Inconel X pipe thermophysical properties were taken from [24].

From the 52 cases presented by Grele and Gedeon, 10 specific cases were simulated, and encompass the range of operating conditions encountered by the experimentalists. The key parameters taken from the experimental data were:

- For the fluid: the velocity inlet, the temperature inlet.
- For the solid: using Equation 5.1, taking the inlet and outlet temperature, the uniform volu-

metric heat flux was calculated and imposed as a cell zone condition.

The 10 cases selected for the simulations are shown in Table 6.1.

Table 6.1: Important input parameters for the ten modelled cases

Case number	V^{Avg} **(m/s)**	T_{in} **(K)**	T_{out} **(K)**	Q^{xy} **(W)**	**Re range**	**Pr range**
8	3.16	854	868	Equation 5.1	6,160-9,160	10.2-14.7
10	3.46	868	893	Equation 5.1	7,570-11,200	9-12.8
19	2.08	862	876	Equation 5.1	4,250-6,300	9.7-14
29	4.23	858	877	Equation 5.1	8,570-12,700	9.7-14
30	3.61	850	864	Equation 5.1	6,840-10,200	10.5-15.2
40	4.26	972	990	Equation 5.1	15,200-22,400	5-7.6
43	3.95	989	1007	Equation 5.1	14,800-22,300	4.6-7.2
44	3.60	991	1012	Equation 5.1	13,600-20,600	4.5-7.1
45	3.20	975	999	Equation 5.1	11,600-17,200	4.8-7.5
46	2.65	985	1013	Equation 5.1	9,950-15,000	4.5-7.2

For clarification, the range for the Reynolds and Prandtl numbers observed in column 6 and 7 of Table 6.1 corresponded to the minimum and maximum values using the aforementioned different combination of thermophysical properties.

Taking into account the two correlations for density, the two correlations for specific heat and the four correlations for viscosity, the total amount of 16 simulations were run per case, yielding a total of 160 simulations. Thus, in order to proceed in a practical way, a loop which went

through all of the possible combinations was programmed in Scheme language, a language seamlessly interpreted by Fluent. In this script, the case was initialized, the properties were changed accordingly, the simulation was run and finally results were exported. Using Matlab, a table containing all the pertinent results was created automatically. In particular, this code calculated the heat transfer coefficient and compared it with Dittus-Boelter and Sieder Tate correlation, both of which use Reynolds and Prandtl numbers as inputs, and therefore a spread exists in that data as well due to dependence on thermophysical properties. Unsurprisingly, the Nusselt number spread using the Sieder Tate correlation was smaller in comparison to that using the Dittus Boelter correlation. On average, the simulation results showed a 1.4% difference when compared to the Sieder Tate correlation and a 4.9% of the Dittus Boelter correlation. This showed that the variation of the viscosity values at the wall surface with respect to the bulk viscosity was significant and could not be neglected.

6.2 Results

The results for the averaged outer wall temperature are shown in Figure 6.1. On the y-axis, the difference between the experimental results and the simulation results for the averaged wall temperature was plotted. The x-axis denotes the specific case number as previously noted.

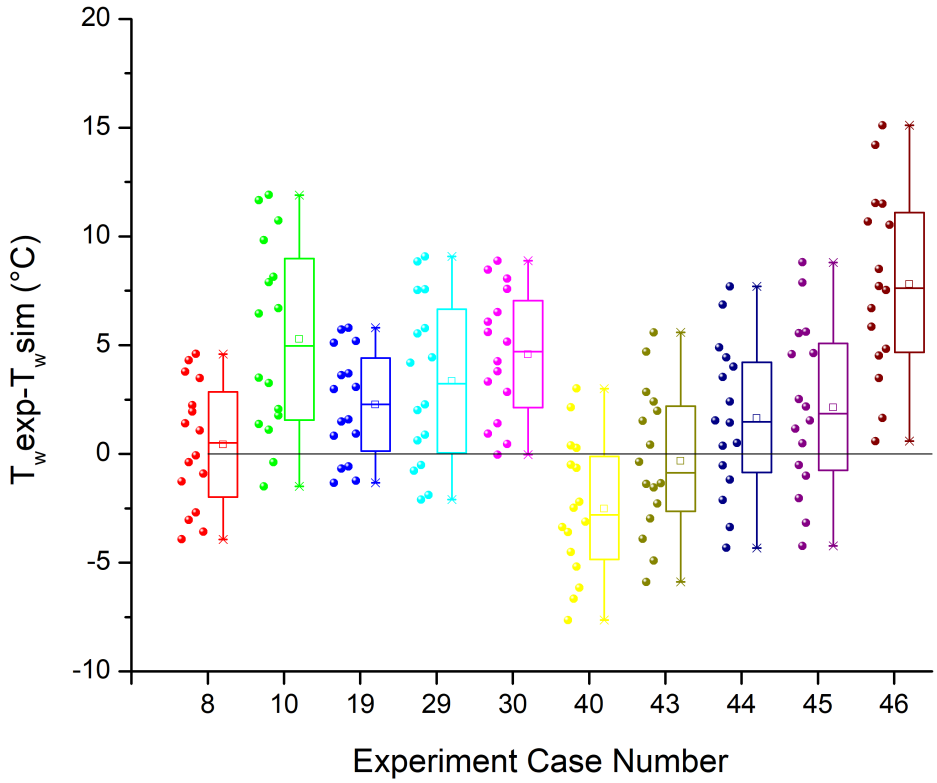

Figure 6.1: Difference between the wall temperature measured in the experiment and the wall temperature resulting from the simulations for each of the ten cases. The various data points in each case correspond to different selections of material properties of FLiNaK

The most noticeable conclusion from Figure 6.1 is that the variations on the predicted thermophysical properties can lead to a wall temperature spread of almost 15 °C. The constant line with a zero value represents the match between the simulation and the experimental results.

Figure 6.2 shows the axial temperature profile of the CFD simulations compared to the measurement of the thermocouples in the external wall for case number 43. It is worth noting that thermocouples readings were shown for only 3 cases in [3]. As can be seen in the figure, the temperature distribution suggests the heat source is not uniform as it drops in the middle of the test

section. However, it is not possible to recreate the experimental conditions given the lack of further details. Figure 6.2 shows the best combination of thermophysical properties along with the two combinations that represent the bounding cases. It can be seen that the uniform volumetric heat source approach is valid, especially with a lack of rationale for choosing a less standard approach to applying the thermal energy.

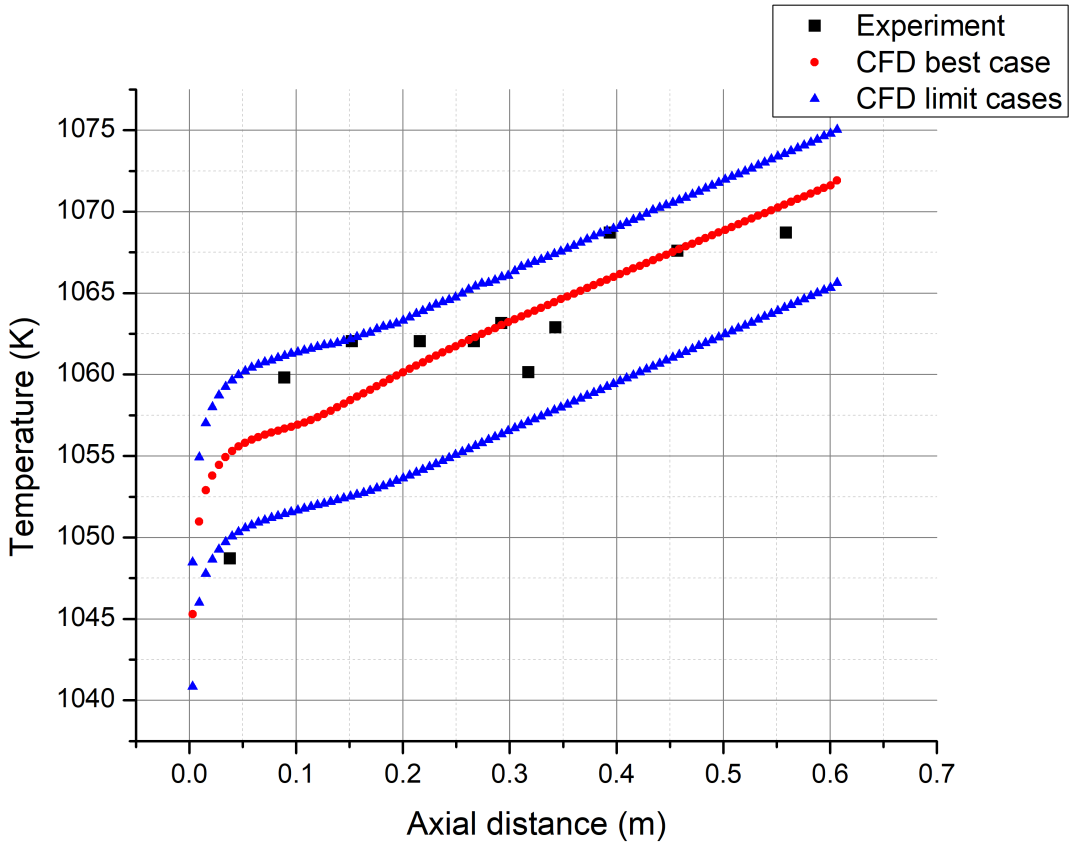

Figure 6.2: Axial temperature on the outer wall of the test section measured with thermocuples in [3] and obtained in the simulations for case 43.

6.3 Remarks

The initial thought with running these experiments was to identify the set of material properties that best describe the experimental results. The properties' correlations that best describe the experiment were not consistent between any two experiments, meaning that the best set of material properties could not be found. It should be noted that even though for some cases (e.g., 30 and 46), results suggest that there is no overlap between experimental results and simulation results, the reader should bear in mind that experimental uncertainties were not reported and cannot accurately be accounted for at this stage.

Due to the aforementioned spread in the wall temperature values, it was observed that the uncertainty in the material thermophysical properties could lead to a significant variance in the heat transfer properties of FLiNaK. This uncertainty coming from the material properties, added to the lack of reliable estimates of experimental uncertainties, impeded an appropriate validation of RANS models for molten salt flows.

Combining the existent considerable variation in the thermophysical properties of FLiNaK present in literature and the temperature spread that this variation may cause, a sensitivity analysis on how the uncertainties in the properties' values affect heat transfer is deemed necessary in order to support future experiments. This sensitivity analysis would help to quantify what is the effect of the uncertainty in the measurement of a certain material property on the heat transfer characteristics of the molten salt.

7. SENSITIVITY ANALYSIS OF THE THERMOPHYSICAL PROPERTIES

7.1 Formulation

A widely used parameter to measure the sensitivity of a simulation result *S(X)* to changes in a parameter X_i is termed as the sensitivity coefficient, whose definition is the following:

$$\text{Sensitivity coefficient} = \frac{\partial S(X)}{\partial X_i} \tag{7.1}$$

where X_i is one element of the vector $\overline{X}$, which includes all dependencies of the variable *S*.

Using a Taylor series approximation, the uncertainty of a function *S(X)* with *n* uncorrelated parameters can be accounted for by using the following expression:

$$u_s = \sqrt{\sum_{n=1}^{\infty} \left(\frac{\partial S(X)}{\partial X_i} . \delta X_i \right)^2} \tag{7.2}$$

For simple cases of an algebraic model, these sensitivity coefficients may be calculated analytically. However, the most common case is that the model is a complex numerical simulation where no algebraic model can be used. Using this analysis as an example, a change in one of the material properties may produce a change in the velocity profile of the fluid and also in the heat transfer properties between the liquid and the solid. Because of the existence of these mentioned coupled effects, the sensitivity coefficient was calculated with data from computational fluid dynamics simulations.

7.2 Procedure

The procedure used in this section was to run the simulation with nominal values of the parameter vector $\overline{X}$. For the next simulations, perturbed values for the input parameter X_i are used. Finally, using a forward finite difference approximation in the parameter space, the sensitivity coefficient is calculated as follows [25]:

$$\frac{\partial S(X)}{\partial X_i} = \frac{S(X_1, X_2, ..., X_i + \Delta X_i, ..., X_n) - S(X_1, X_2, ..., X_i, ..., X_n)}{\Delta X_i} \tag{7.3}$$

For this particular case, the simulation result of interest *S(X)* was the heat transfer coefficient between the molten salt and the solid pipe. The vector of parameters $\overline{X}$ consisted of the four thermophysical properties of FLiNaK.

It is worth pointing out that the One Factor At a Time Approach [26] was used in the following analysis. In this approach, only one parameter changes its value between consecutive simulations, and so, in a deterministic model, the analyst can determine exactly what effect is caused by changing the parameter. In order to obtain good results, the model must be linear in the sense that Gaussian distributions are assumed between input and output values. In addition, there should not be a significant covariance between the input parameters of the sensitivity analysis. Even though it is known that the thermophysical properties are related to similar underlying molecular mechanisms [27] and that the model may have non-linear effects, the current analysis presents a first approach to sensitivity analysis in molten salt flows. Therefore, for the sake of simplification, the model response is assumed linear and that the covariance is not significant. Additional studies should be conducted in the future to validate this claim.

Taking into account every correlation presented in Table 2.1, an average temperature dependent

function was calculated for each property. In order to do this, the temperature dependent expression for each property was evaluated at each temperature in the range of 800-1100K. Next, these values were averaged, yielding one average value of the property for each temperature. Finally, a fitting analysis was made to obtain the average function which better described the behaviour of the material property in question (see Figure 7.1). From this point onwards, in each one of the simulations, only one of the properties was varied while keeping this same functional shape obtained in the fitting. The variations for the analysis were constant steps and the range of these variations was in agreement with respect to maximum and minimum values of the property of interest, as it is shown in Figure 7.2. The remaining average temperature dependent properties were kept invariant for each analysis. As an example, the input viscosities for the sensitivity analysis are shown in Figure 7.2.

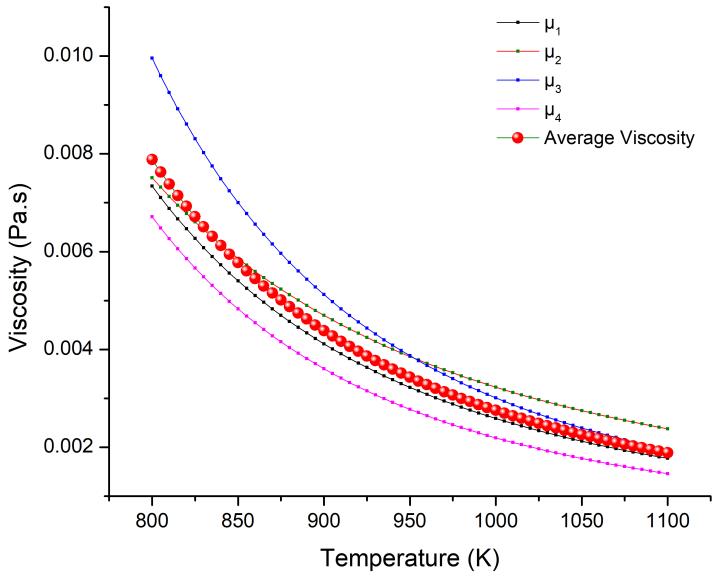

Figure 7.1: Temperature dependent correlations for viscosity and the average viscosity function obtained by exponential fitting.

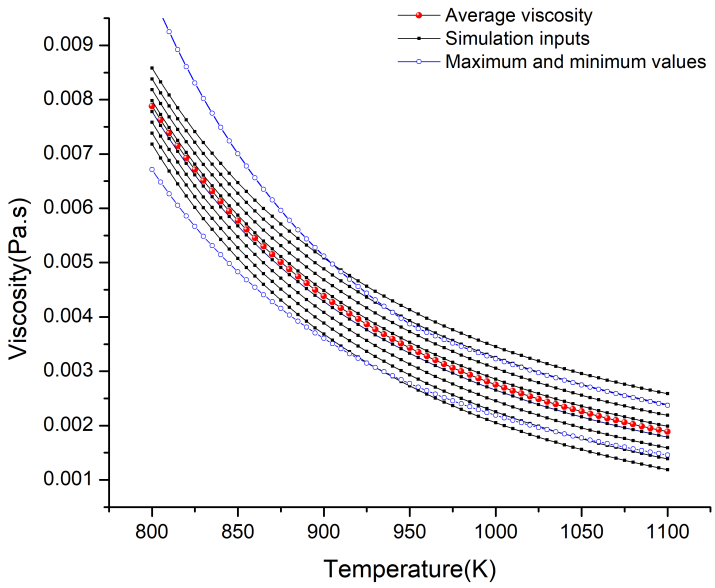

Figure 7.2: Viscosity inputs for the sensitivity analysis CFD simulations.

In Figure 7.1 the four models for viscosity in addition to the average viscosity in the temperature range of interest are plotted. From Figure 7.2, the average viscosity function and the simulation inputs for the sensitivity analysis can be observed. An analogous process of obtaining an average function and adding constant steps to build the simulation inputs was done for the density, the thermal conductivity and the specific heat. Particularly for the thermal conductivity case Smirnov's correlation [8] (shown in Table 2.1) was used, and the variations were done according to the studies done by Williams et al. [13], which states that the values should range between $0.6\frac{W}{m\cdot K}$ and $1.0\frac{W}{m\cdot K}$ at 973 K.

As it was mentioned before, the sensitivity analysis in this section was targeted at obtaining sensitivity coefficients for the heat transfer coefficient variable. Thus, each one of the eight black curves labeled as Simulation Inputs in Figure 7.2 were used in the simulations in order to obtain

the corresponding heat transfer coefficients as a function of the property value evaluated at the bulk temperature. The simulations were done in three different temperature ranges, determined by different temperature inlet boundary conditions. Hence, some of the typical temperatures of operation present in a MSR were covered.

7.3 Sensitivity Analysis Results

The resulting heat transfer coefficients obtained in the simulations as a function of viscosity, density, specific heat and thermal conductivities are plotted in Figures 7.3, 7.4, 7.5, 7.6. Taking as an example the viscosity sensitivty analysis, from Figure 7.6 it can be observed that there are eight different values of heat transfer coefficients for each temperature range. This matches the number of simulation inputs described in Figure 7.2.

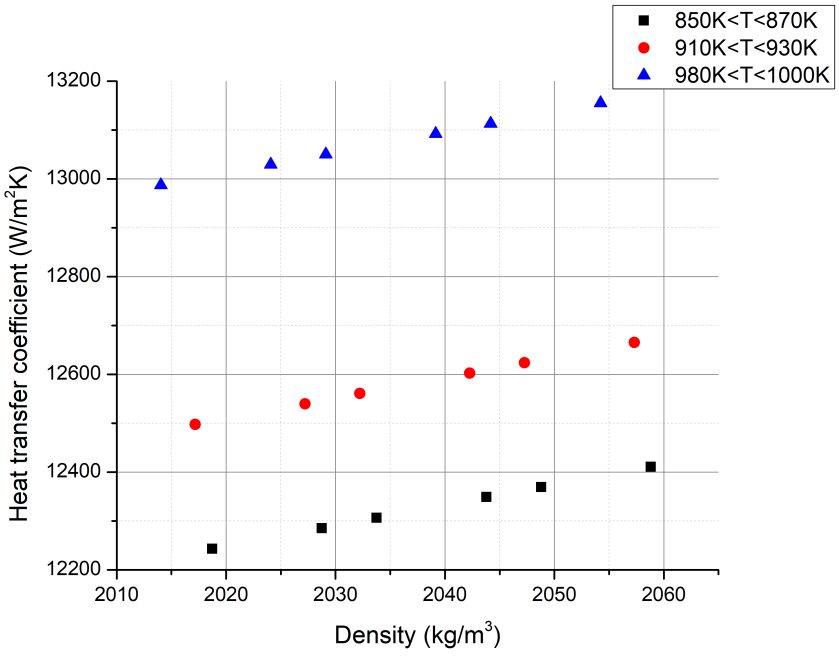

Figure 7.3: Heat transfer coefficients versus density variations.

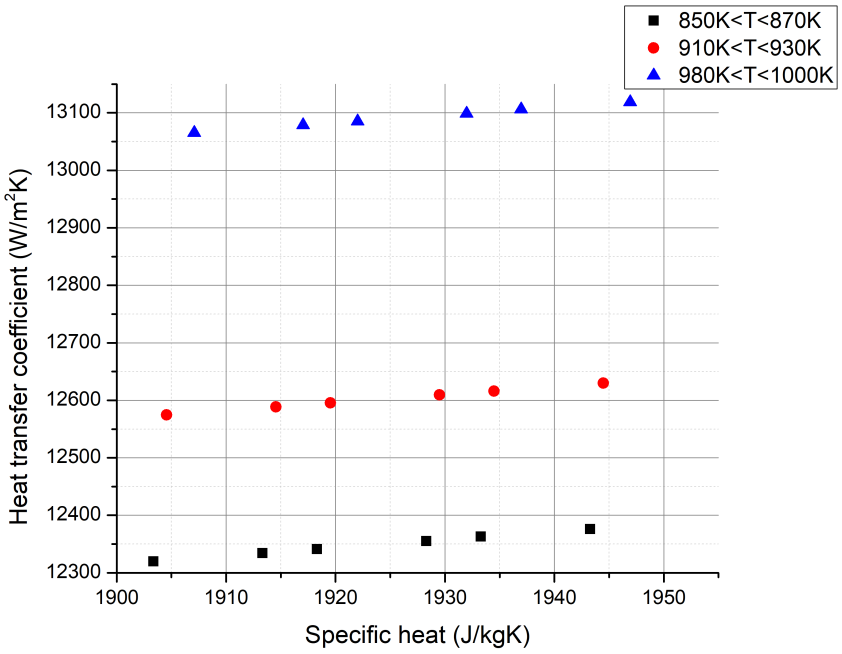

Figure 7.4: Heat transfer coefficients versus specific heat variations.

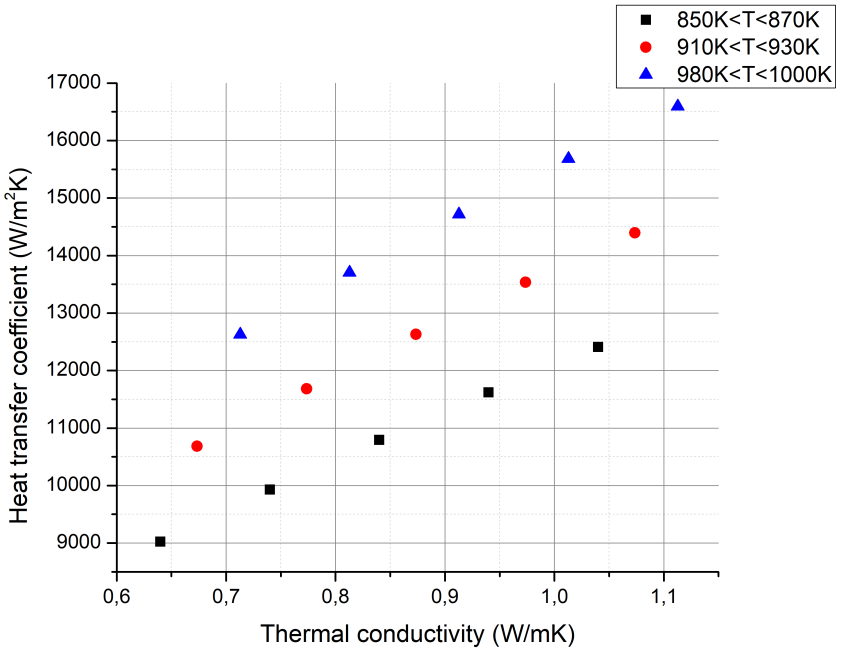

Figure 7.5: Heat transfer coefficients versus thermal conductivity.

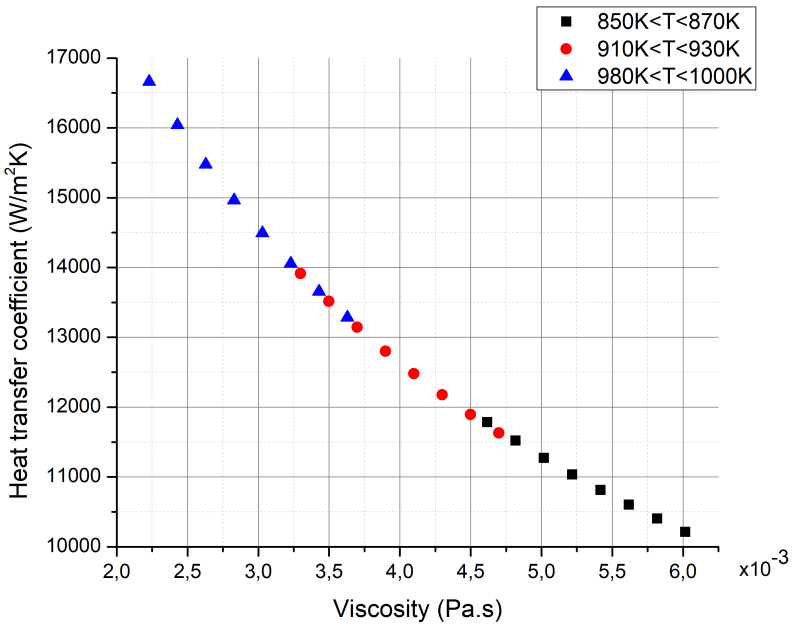

Figure 7.6: Heat transfer coefficients versus viscosity.

From the data shown in the previous Figures , the results of the calculation of the sensitivity coefficients for different temperature ranges are shown in Table 7.1.

Table 7.1: Sensitivity coefficients for each property in different temperature ranges

Material property	**850K<T<870K**	**910K<T<930K**	**980K<T<1000K**
Viscosity	(-1.112 $\pm$ 0.036) 10^6 $\frac{J}{m.K.kg}$	(-1.627 $\pm$ 0.045) 10^6 $\frac{J}{m.K.kg}$	(-2.398 $\pm$ 0.084) 10^6 $\frac{J}{m.K.kg}$
Density	(4.188 $\pm$ 0.012) $\frac{W.m}{K.kg}$	(4.180 $\pm$ 0.009) $\frac{W.m}{K.kg}$	(4.178 $\pm$ 0.002) $\frac{W.m}{K.kg}$
Specific heat	(1.410 $\pm$ 0.017) $\frac{kg}{m^2.s}$	(1.384 $\pm$ 0.002) $\frac{kg}{m^2.s}$	(1.355 $\pm$ 0.009) $\frac{kg}{m^2.s}$
Thermal conductivity	(8.458 $\pm$ 0.129) 10^3 $\frac{1}{m}$	(9.267 $\pm$ 0.159) 10^3 $\frac{1}{m}$	(9.908 $\pm$ 0.188) 10^3 $\frac{1}{m}$

Note that the sensitivity coefficient is positive for three of the four properties considered with viscosity alone having a negative value. This is not surprising since an increase in viscosity would

decrease the Reynolds number, thereby diminishing the amount of turbulence as well as the transfer of thermal energy.

Nusselt number calculations using Dittus Boelter and Sieder Tate correlations were performed in order to compare and assess the validity of using both of these correlations. The comparison was done using the results for the viscosity sensitivity analysis, which was a representative case (see Figure 7.7).

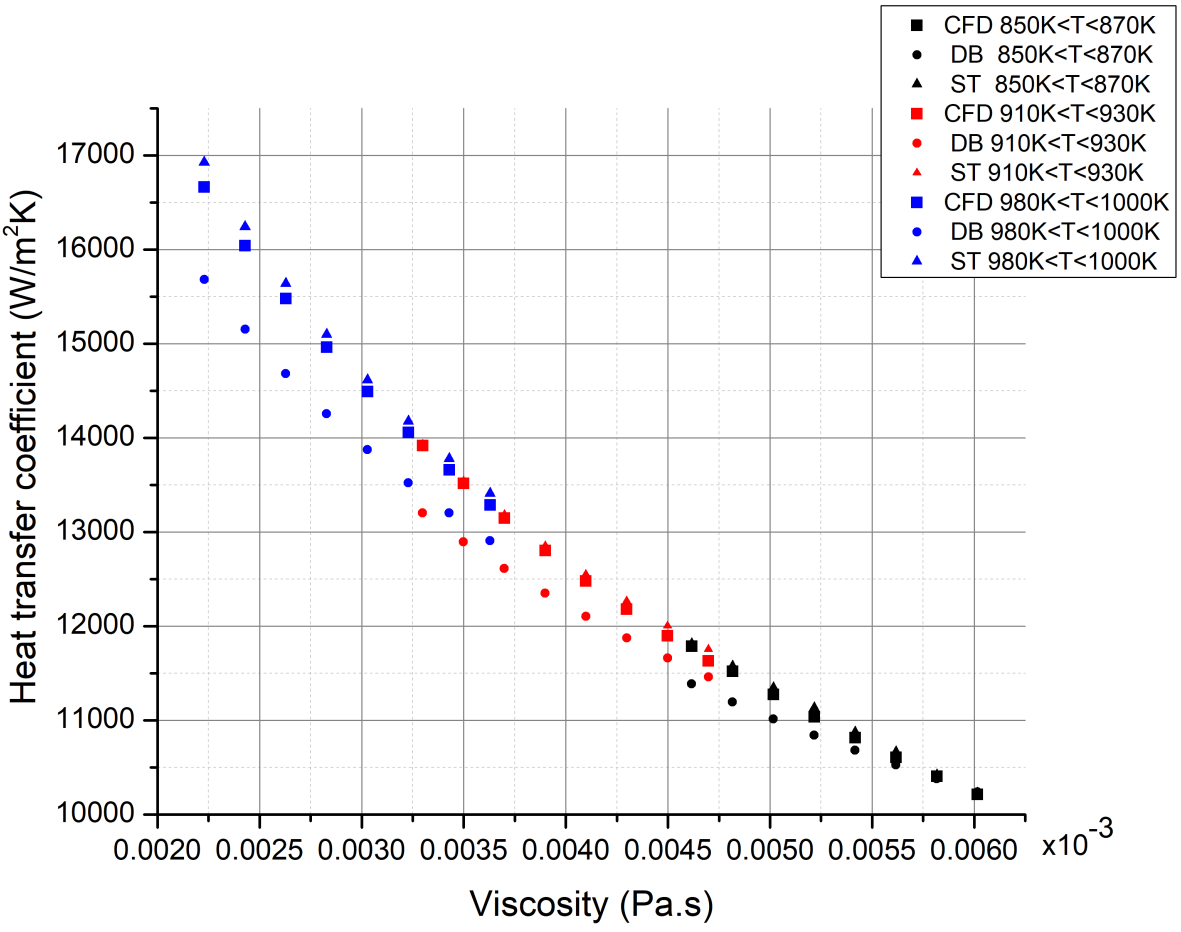

Figure 7.7: Heat transfer coefficient versus thermal conductivity values obtained from the sensitivity analysis. Comparisons with Dittus Boelter and Sieder Tate were made.

As it can be seen from Figure 7.7, Sieder Tate predictions agree much better with CFD simulation results compared to Dittus Boelter. This is not surprising in that the Sieder Tate formula accounts for the variability in fluid properties near the wall, which can influence the heat transfer performance. The slope of the curves in Figure 7.7 also reveal a good agreement between Sieder Tate and our CFD simulations suggesting similar sensitivity from the viscosity on the heat transfer coefficient could be predicted based on the Sieder Tate correlation. It is important to note that the CFD simulations allow a direct calculation of the surface temperature, and therefore provide the evidence of the validity of the Sieder Tate formula in this scenario. Additional work should be performed with other turbulence models and higher fidelity simulations to more completely establish this validity.

Apart from the sensitivity coefficients presented above in Equation 7.3, a dimensionless sensitivity parameter is an alternative way to provide information about how a certain parameter affects the variable of interest. Consequently, the dimensionless sensitivity coefficient is defined as:

$$S^* = \frac{\frac{\delta h}{h}}{\frac{\delta x}{x}} \tag{7.4}$$

Equation 7.4 suggests a rather simple interpretation for S^*, namely a fractional variation in the calculated observable quantity (in this case the heat transfer coefficient) that is produced by a specific fractional change in a selected input parameter (in this case material properties). In Equation 7.4, the observable quantity *h* is defined as the heat transfer coefficient values obtained by using the average values of the material properties *x*. For the viscosity sensitivity analysis, the heat transfer coefficient *h* appearing in Equation 7.4 would be calculated with the average viscosity red curve in Figure 7.2 and the remaining property average values. The amount of variation of *x*

is δx while the resulting change in h is δh. Using these definitions, the dimensionless sensitivity coefficients were calculated and are presented in Table 7.2. Also, the maximum variations in percentage of a material property from the mean value according to the different correlations can be observed.

Table 7.2: Dimensionless sensitivity coefficients for each property, and their respective maximum variation determined by the different correlations

Parameter	S^*	**Maximum percent variations between correlations**
Viscosity	-0.51 $\pm$ 0.07	~18%
Specific Heat	0.21 $\pm$ 0.01	~5%
Density	0.67 $\pm$ 0.02	~1%
Thermal Conductivity	0.64 $\pm$ 0.03	~26%

According to the results shown in Table 7.2, viscosity, thermal conductivity and density have the highest dimensionless sensitivity coefficient. Nevertheless, the percentage change in density among the correlations is very small compared to the thermal conductivity and viscosity, making it less relevant in terms of how it might affect the prediction of the heat transfer coefficient. This is due to the fact that the determination of the value of density is a less complex task than the measurement of the other two properties. In contrast, the thermal conductivity values reported by [7] and [13], may vary between 0.6 and 1.0 W/mK approximately, which accounts for a maximum of 26% spread, measured from the average value at a specific temperature.

Therefore, to be able to producing high quality experimental data for future validation purposes, a more confident understanding of material properties is fundamental. More specifically to future molten salt efforts, thermal conductivity and viscosity need to be accurately described since they

are the most sensitive parameter.

8. CONCLUSION

Reynolds averaged Navier Stokes using the k-ω SST model was used to perform computational fluid dynamics simulations attempting to reproduce the experiment results obtained by Grele & Gedeon [3] in 1954. Lack of detail and uncertainty estimates of the experimental data prevented a full validation effort. Despite the inability to conducting full validation studies, the influence of the variation of the thermophysical properties was gauged as they pertained to external wall temperatures and heat transfer coefficients. A large spread of values was observed for the external wall temperature of the simulations.

In light of the uncertainty of FLiNaK's thermophyisical properties, a sensitivity analysis using a one-factor at a time approach was done to account for the influence of these variations on the heat transfer coefficient for each one of the properties. The analysis proved that viscosity and thermal conductivity are the most crucial properties for conjugate heat transfer simulations using FLiNaK. The simulations also demonstrated that Sieder Tate correlation can be used with a reasonable level of trust since the results agreed well with that expression. It is not surprising that the Dittus Boelter expression did not agree as well, especially considering it cannot account for different viscosity at the wall compared to the bulk. This considered analysis can be extended to other molten salts due to the similarity in the dimensionless numbers (Prandtl and Reynolds) used in the study.

This work provides evidence on the importance of conducting further research in the material properties for FLiNaK, as they have a significant effect in the prediction of the heat transfer coefficient. Additional turbulence models should also be run to further validate the use of the Sieder Tate correlation and gain further insight into the flow physics.

For future studies, a sensitivity analysis using Large Eddy Simulations (LES) and DNS is suggested with the aim of reducing the impact arising from the error in the turbulence model used and the assumptions built into those models. In addition, it is important to note that this entire analysis was based on main effects of the material properties. Further studies to quantify any interactions between the variations of more than one property at the same time are suggested. This potential analysis would serve to quantify the covariance between the uncertainty of two properties. In this way a probability density functions of inputs and outputs in the current sensitivity study could be characterized in order to obtain the non-linearity effects of the thermophysical properties' effect on the heat transfer coefficient.

REFERENCES

[1] H. Bussier, S. Delpech, V. Ghetta, D. Heuer, D.E. Holcomb, V. Ignat'ev, E. Merle-Lucotte, J. Serp. "The molten salt reactor (MSR) in generation IV: overview and perspectives". Progress in Nuclear Energy, 77, 308-319. (2014).

[2] Mauricio Tano Retamales. Developement of multi-physical multiscale models for molten salts at high temperature and their experimental validation. Nuclear Experiment [nucl-ex]. Université Grenoble Alpes, 2018.

[3] M.D. Grele, L. Gedeon. "Forced-convection heat-transfer characteristics of molten FLiNaK flowing in an Inconel X system". National Advisory Committee for Aeronautics (1954).

[4] H.W. Hoffman, J. Lones, "Fused Salt Heat Transfer Part II: Forced Convection Heat Transfer in Circular Tubes Containing NaF-KF-LiF Eutectic," ORNL-1977, Oak Ridge National Laboratory (1955).

[5] I. B. Vriesema, "Aspects of Molten Fluorides as Heat Transfer Agents for Power Generation," WTHD No. 112, Delft University of Technology.

[6] V. Ignat'ev et al., "Heat Exchange During the Flow of a Melt of LiF-NaF-KF Fluoride Salts in a Circular Tube", Sov. At. Energy, 57, 2, 123 (1984).

[7] C. T. Ewing et al., "Radiant Transfer of Heat in Molten Inorganic Compounds at High Temperatures," J. Chem. Eng. Data, 7, 2, 246 (1962).

[8] M.V. Smirnov, V.A. Khoklov, E. S. Filatov, "Thermal Conductivity of Molten Alkali Halides and Their Mixtures," Electrochim. Acta, 32, 7, 1019 (1987).

[9] J. Ambrosek, M. Anderson, K. Sridharan, T. Allen . "Current status of knowledge of the fluoride salt (FLiNaK) heat transfer". Nuclear technology, 165(2), 166-173 (2009).

[10] M.S. Sohal, M.A. Ebner, P. Sabharwall, P. Sharpe. "Engineering database of liquid salt thermophysical and thermochemical properties" (No. INL/EXT-10-18297). Idaho National Laboratory (INL) (2010).

[11] Xu, C., Wang, Z., He, Y., Li, X. Bai, F. (2012). Sensitivity analysis of the numerical study on the thermal performance of a packed-bed molten salt thermocline thermal storage system. Applied Energy, 92, 65-75.

[12] B: Sabharwall, P., Kim, E. S., McKellar, M.; Anderson, N. (2011). Process heat exchanger options for the advanced high temperature reactor (No. INL/EXT-11-21584). Idaho National Laboratory (INL).

[13] D.F. Williams, L.M. Toth, K.T. Clarno. "Assessment of Candidate Molten Salt Coolants for the Advanced High-Temperature Reactor (AHTR)", ORNL/TM-2006/12, Oak Ridge National Laboratory, Oak Ridge, TN, (2006).

[14] G.J. Janz, R.P.T. Tomkins. “Physical Properties Data Compilations Relevant to Energy Storage: IV Molten Salts: Data on Additional Single and Multi-Component Salt Systems,” National Standard Reference Data System, National Bureau of Standards Report NSRDS-NBS 61 Part IV (1981).

[15] T. Allen, "Molten Salt Database", http://allen.neep.wisc.edu/shell/index.php/salts, Nuclear Engineering and Engineering Physics Department, University of Wisconsin (2010).

[16] F. Menter. "Zonal two equation kw turbulence models for aerodynamic flows". In 23rd fluid dynamics, plasmadynamics, and lasers conference (p. 2906) (1993).

[17] Kim, W. S., et al. "Performance of a variety of low Reynolds number turbulence models applied to mixed convection heat transfer to air flowing upwards in a vertical tube." Proceedings of the Institution of Mechanical Engineers, Part C: Journal of Mechanical Engineering Science 218.11 (2004): 1361-1372.

[18] F. Menter, J. Carregal Ferreira, T. Esch, B.Konno. "The SST Turbulence Model with Improved Wall Treatment for Heat Transfer Predictions in Gas Turbines". Proceedings of the International Gas Turbine Congress 2003 Tokyo.

[19] D. C. Wilcox. Turbulence modeling for CFD (Vol. 2, pp. 172-180). La Canada, CA: DCW industries (1998).

[20] Chen, Y., Tang, Z., & Wang, N. NUMERICAL PREDICTION OF TURBULENT CONVECTIVE HEAT TRANSFER WITH MOLTEN SALT IN CIRCULAR PIPE.

[21] Ferng, Y. M., Kun-Yueh Lin, and Chen-Wei Chi. "CFD investigating thermal-hydraulic characteristics of FLiNaK salt as a heat exchange fluid." Applied Thermal Engineering 37 (2012): 235-240.

[22] F. Moukalled, L. Mangani, M. Darwish. "The finite volume method in computational fluid dynamics. An Advanced Introduction with OpenFOAM and Matlab", 3-8 (2016).

[23] Chaleff, Ethan S., Thomas Blue, and Piyush Sabharwall. "Radiation heat transfer in the Molten Salt FLiNaK." Nuclear Technology 196.1 (2016): 53-60.

[24] "Inconel X-750 Technical Data". *High Temp Metals*, 2015, www.hightempmetals.com/techdata/hitempInconelX750data.php. Accesed November 2018.

[25] American Society of Mechanical Engineers. "Standard for Verification and Validation in Computational Fluid Dynamics and Heat Transfer: An American National Standard". American Society of Mechanical Engineers (2009).

[26] A. Saltelli et al., Global Sensitivity Analysis, John Wiley; Sons, ISBN 978-0-470-05997-5, 2008.

[27] Gheribi, A. E., Corradini, D., Dewan, L., Chartrand, P., Simon, C., Madden, P. A.; Salanne, M. (2014). Prediction of the thermophysical properties of molten salt fast reactor fuel from first-principles. Molecular Physics, 112(9-10), 1305-1312.